A variable resolution SPH scheme based on independent domains coupling

Francesco Ricci
Department of Mechanical
and Industrial Engineering
New Jersey Institute of Technology
Newark, New Jersey, USA
fr248@njit.edu

Renato Vacondio
Dipartimento di Ingegneria e Architettura
Università degli Studi di Parma
Parma, Italy
renato.vacondio@unipr.it

Angelo Tafuni
School of Applied Engineering
and Technology
New Jersey Institute of Technology
Newark, New Jersey, USA
atafuni@njit.edu

Abstract—Variable resolution in Smoothed Particle Hydrodynamics is essential for simulating several engineering problems characterized by different scales, to the point that this topic is listed as one of the open SPHERIC Grand Challenges [1].

This work presents a new multi-resolution algorithm for weakly compressible Smoothed Particle Hydrodynamics (WC-SPH), where an approach based on a domain-decomposition strategy is adopted. The domain is divided in an arbitrary number of different zones, which are connected only through additional Dirichlet boundary conditions enforced by buffer regions. The physical quantities of SPH particles in the buffers are computed by means of a corrected SPH interpolation over adjacent sub-domains. Specifically, a second-order kernel correction procedure is employed to ensure the proper consistency and accuracy of the interpolation. To model the mass transfer between the sub-domains, a procedure based on the evaluation of the Eulerian mass flux at the domain boundaries is applied. Particles that belong to a specific zone are created/destroyed in the buffer regions and do not interact with fluid particles that belong to a different resolution zone. One major strength of the presented multi-resolution strategy is that there is virtually no limit to the number of resolution levels that can be deployed, therefore this new model is ideal for simulating multi-scale applications.

The algorithm has been implemented in the DualSPhysics opensource code [2] and optimized thanks to DualSPHysics' parallel framework. The algorithm has been tested on a series of different cases, showing promising results for both internal and freesurface flows.

I. Introduction

In the last few decades, the Smoothed Particle Hydrodynamics (SPH) method, originally proposed for astrophysical application [3], has been extended to the simulation of freesurface [4], multi-phase flows [5] such as those recurring in coastal and ocean engineering applications, as well as fluid-structure interaction problems [6]. Compared grid-based methods, which employ costly computational techniques such as Level-Set [7], Volume of Fluid(VOF) [8] and front-tracking techniques [9], often coupled with Adaptive Mesh Refinement (AMR) technique, due to his Lagrangian formulation the SPH method can efficiently handle complex evolving interfaces. However, one weakness with respect to mesh-based methods is that it is challenging to vary the spatial resolution locally. Among other reasons, the smoothed nature of the method

prevents a sharp variation of the particle size, and the isotropy of the kernel interpolation impedes increasing the resolution in a preferred direction. Furthermore, the interaction between particles of different sizes must be carefully treated to avoid the introduction of error in the SPH spatial operators.

Historically, early attempts for the introduction of adaptivity in the SPH method were focused on the introduction of a variable smoothing length formulation coupled with the definition of regions with different particle sizes at the beginning of the simulations [10]–[13].

Instead, later efforts aimed to dynamically increase the particle resolution by introducing a refinement process under the constraints of conserving mass, momentum, and angular velocity and minimizing the error in the estimation of the density [14], [15]. This approach is coupled in [16] to a derefinement process based on coalescing particles with similar sizes and extended to 3D [17]. Instead, in [18] a different approach based on the particle equivalent of the AMR technique has been proposed, which has been improved [19] by introducing "buffer" layers. Using this approach, in [20] results are presented for flows past bodies with various shapes.

An approach based on multi-decomposition has been proposed in [21], however, the results presented only two levels of refinement, and the density formulation wasn't able to treat free-surface flows. Multi-resolution approaches, mainly devoted to Fluid-Structure interaction problems, in which different resolutions are defined between the fluid and the solid phase, have been proposed in [22] and [23].

The main aim of this work is the development of a robust and efficient adaptive resolution approach within the SPH method. The proposed algorithm has been implemented into the open-source SPH solver DualSPHysics [2].

The approach is based on the decomposition of the computational domain in different sub-domains, each with its characteristic particle size and smoothing length. At each time step, the Navier-Stokes equations are solved independently in every sub-domain, for which the closure is provided by a buffer region that acts as a Dirichlet boundary condition. The coupling between different domains is obtained by reinterpolating the physical quantities at buffer particles using

the information available at the fluid particles of the adjacent domains. To ensure the consistency of the interpolation, a 2nd order kernel correction procedure is adopted, together with a regularization procedure in the buffer regions based on the Particle Shifting Technique. The mass transfer between subdomains is taken into account by evaluating the Eulerian mass flux at the domain boundaries following a procedure similar to the one adopted in [24].

The rest of the paper is organized as follows: in Section II, the proposed multi-resolution algorithm is presented, whereas in Section III, a brief introduction of the SPH method is provided. In Section IV the variable resolution approach is validated against a flow past a cylinder for different Reynolds numbers, a flow past a moving cylinder with forced motion in the cross-flow direction, and propagation of regular waves in a rectangular tank. In Section V, conclusions are drawn and future research area is illustrated.

II. MULTI-RESOLUTION ALGORITHM

The proposed variable resolution algorithm is based on a domain decomposition approach, so that computational domain Γ is partitioned in a set of N sub-domains Γ_i such that $\Gamma = \bigcup_{i=1}^N \Gamma_n$, with each sub-domain characterized by its characteristic particle size dp_i and smoothing length h_i . In order to solve the computational problem from t^n to t^{n+1} , a closure in the form of Dirichlet boundary condition must be provided at the boundaries of each sub-domain Γ_i . For this purpose, each sub-domain is extended by a buffer region $\partial \Gamma_i$ with width $l_{\partial \Gamma_i} = 2h_i$.

The buffer particles located close to the interface have their support truncated, therefore the corrected SPH interpolation proposed in [25] is employed to ensure consistency. The last part of the algorithm regards the exchange of mass between the different sub-domains. In the proposed approach, at the beginning of the time step the following conditions are checked:

- 1) If a *buffer particles* moves into the fluid domain, it is transformed into a *fluid particle*.
- 2) If a *fluid particle* enters the buffer region, it becomes a *buffer particle*.
- 3) If a buffer particles moves outside the extended subdomain $\partial \Gamma_i \cup \Gamma_i$ is deleted.

For the particle insertion, we instead employ the following procedure. The external boundary of the sub-domain i is divided into a mass segments with a length equal to the characteristic size dp_i of the sub-domain Γ_i . At each time step we calculate the Eulerian mass flux across the segment using a mid-point rule, such as:

$$F_{m_a} = \max(0.0, \rho_{m_a}(v_{m_a} - v_{b_f}) \cdot \mathbf{n} dp_i dt) \tag{1}$$

where F_{m_a} is the mass flux during the time step dt, ρ_{m_a} and v_{m_a} are the density and the velocity calculated at the mass accumulation point using the same SPH corrected interpolation employed for the *buffer particles* and v_{b_f} is the velocity of the interface. After F_{m_a} is added to m_a if $m_a \geq (dp)^D/\rho_0$, where

D is the dimensionality of the problem, a particle is inserted in the buffer region at a distance equal to dp/2 in the normal direction at the interface.

Buffer particles move accordingly to their Lagrangian velocity (obtained by interpolation from the couples sub-domain) and, differently from the fluid particles, the buffer ones do not interact with each other. This can lead to a highly irregular particle distribution in the buffer areas, which is obviously undesired. To solve this issue, the *buffer particles* position is regularized with a procedure based on the Particle Shifting Technique (PST).

III. METHODOLOGY

THe SPH discretization of the weakly compressible Navier-Stokes equations is :

$$\frac{D\rho}{Dt} = \rho_a \sum_b (\mathbf{v}_a - \mathbf{v}_b) \cdot \nabla_a W_{ab} V_b + \mathcal{D}_a \tag{2}$$

$$\frac{D\mathbf{v}}{Dt} = -\frac{1}{\rho_a} \sum_b (p_a + p_b) \nabla_a W_{ab} V_b + \mathbf{f}_a + \Pi_a \qquad (3)$$

$$\frac{D\mathbf{x}}{Dt} = \mathbf{v} \tag{4}$$

where ρ is the density, ${\bf x}$ is the position, ${\bf v}$ is the velocity, ${\bf g}$ is the gravity, P is the pressure, ${\cal D}_a$ and Π_a are the diffusion terms respectively for the continuity and the momentum equation, ${\bf f}_a$ is the volume forces and W_{ab} is the SPH kernel function. As a closure, a barotropic relation between the density and the pressure is employed to keep the maximum density variation in the range of 1% of the reference density. In this work has been used the Wendland [26] kernel C2.

As for the Density Diffusion Term (DDT) \mathcal{D}_a , the formulation by Fourtakas [27] is chosen.

For laminar flow the viscous stress formulation of Shao & Lo [28] is adopted:

$$\Pi_a = \sum_b 4m_b \frac{\nu(\mathbf{x}_a - \mathbf{x}_b) \cdot \nabla_a W_{ab}}{(\rho_a + \rho_b)||\mathbf{x}_a - \mathbf{x}_b)||^2} (\mathbf{v}_a - \mathbf{v}_b)$$
 (5)

where ν is the kinematic viscosity of the fluid.

Whereas, the artificial viscosity is instead adopted for gravity-dominated fluid:

$$\Pi_{a} = \begin{cases}
\sum_{b} 2m_{b} \frac{\alpha h c_{0} \mu_{ab}}{\rho_{a} + \rho_{b}} \nabla_{a} W_{ab}, & (\mathbf{v}_{a} - \mathbf{v}_{b}) \cdot (\mathbf{x}_{a} - \mathbf{x}_{b}) < 0 \\
0, & (\mathbf{v}_{a} - \mathbf{v}_{b}) \cdot (\mathbf{x}_{a} - \mathbf{x}_{b}) > 0
\end{cases}$$
(6)

where

$$\mu_{ab} = \frac{(\mathbf{v}_a - \mathbf{v}_b) \cdot (\mathbf{x}_a - \mathbf{x}_b)}{|\mathbf{x}_a - \mathbf{x}_b)||^2}$$
(7)

The solid boundary modeling is based on the modified Dynamic Boundary Condition (mDBC) proposed in [29]. No-slip conditions are enforced at the solid boundaries, following the approach outlined in [30].

To regularize the particle distribution is the Particle Shifting Technique [31] is employed. The magnitude of the shifting is modeled with a Fickian law:

$$\delta \mathbf{x} = -D\nabla C \tag{8}$$

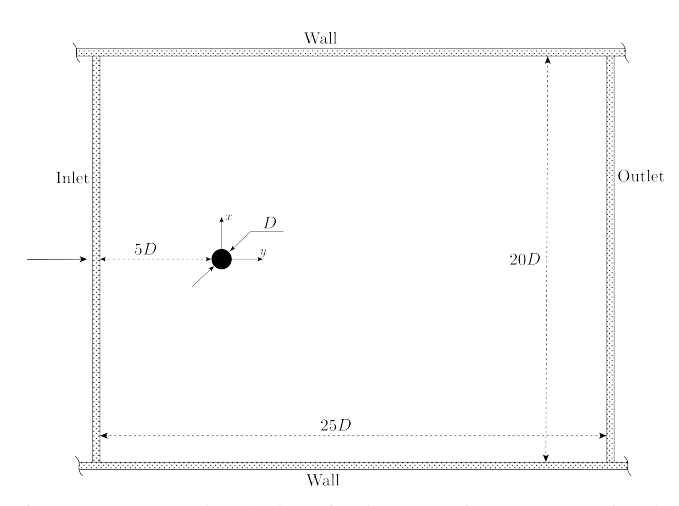


Fig. 1: Computational domain for 2-D flow past a circular cylinder.

where D is the diffusion coefficient defined as:

$$D = Ah^2. (9)$$

Here, A is a dimensionless constant that is tuned based on the particular problem and dp is the particle size. The gradient of concentration ∇C is calculated using an SPH discretization of the gradient given by:

$$\nabla C = \sum_{b} \frac{m_b}{\rho_b} \nabla W_{ab}.$$
 (10)

In this work a second-order symplectic predictor-corrector [32] is employed as time scheme.

IV. RESULTS AND DISCUSSION

A. Flow past a circular cylinder

To evaluate the proposed approach, the flow past a circular cylinder for several Reynolds numbers Re is simulated. The computational domain, shown in Figure 1, is chosen in accordance to [24]: the cylinder with diameter D = 0.1m is centered at (x,y) = (0,0) while the computational domain has a dimension of $25D \times 20D$ that ensure the absence of any blockage effect. No-slip solid boundary conditions are imposed at the cylinder, while free-slip conditions are defined at the bottom and upper wall. Inflow-outflow conditions are imposed using the formulation proposed in [24]: at the inlet the velocity and the density are imposed, whereas at the outlet the velocity is extrapolated from the fluid to the buffer region, while the density is fixed at the reference value. The fluid is initialized with $U_{\infty}(x,y) = (1,0)$ m/s while the density has an initial value equal to $\rho_0 = \rho_\infty = 1000 \text{ kg/m}^3$. The Reynolds Number Re= $U_{\infty}D\nu^{-1}$ is varied by changing the value of the kinematic viscosity ν . The smoothing-length is set equal to $h = 2\Delta x$, constant across the different sub-domains, the DDT in Equation 5 is employed, and Particle Shifting is applied to avoid the creation of empty regions due to the vortical structures that develop in the wake.

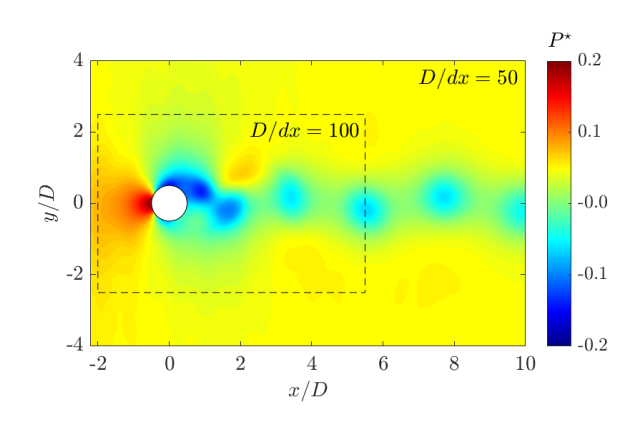


Fig. 2: Dimensionless pressure field for a flow past cylinder with Re=200.

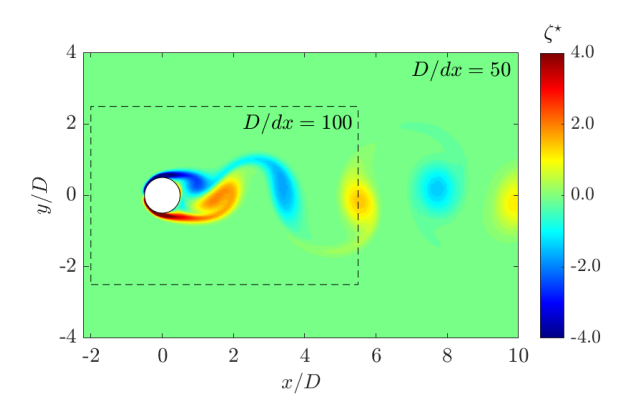


Fig. 3: Dimensionless vorticity field for a flow past cylinder with Re=200.

1) Re=200: The unsteady flow past a circular cylinder with 200 is computed. The computational domain is discretized in three different sub-domains with particle spacing equal to $D/\Delta x=25,50,100$. The refinement regions are centered at the cylinder and extended downstream to better resolve the wake region. The dimensionless pressure and Dimensionless vorticity contours $\zeta^{\star}=\zeta(x/D,y/D)DU^{-1}P^{\star}=P(x/D,y/D)\rho^{-1}U_{\infty}^{2}$ are shown respectively in Figure 2 and Figure 3 and it can be noted that no discontinuities are visible through the interface between the fine and the medium refinement regions, demonstrating the robustness of the coupling between sub-domains.

To quantitatively assess the results the drag and lift coefficients C_D , C_L , and the Strouhal number St have been computed. In Figure 4 the time history of C_L and C_D , is shown. The mean values of the drag and lift coefficient and the Strouhal number are reported in Table I and compared to other relevant SPH studies, a close agreement between the

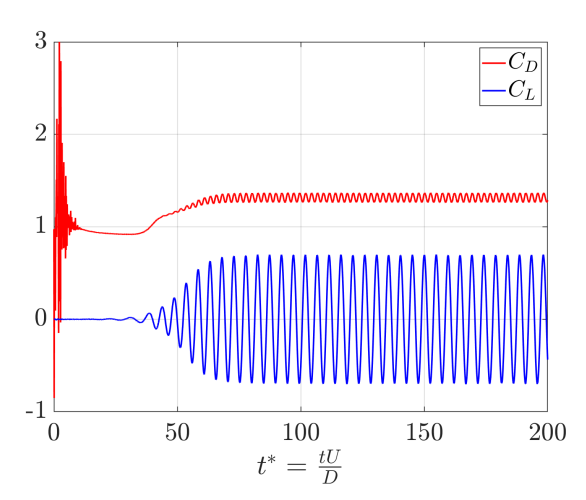


Fig. 4: Time history of the drag and lift coefficient for a flow past cylinder with Re=200.

Re		Present	Tafuni et al. [24]	Liu et al. [33]	Marrone et al. [30]
200	C_D C_L St	1.316 0.7 0.205	1.46 0.693 0.206	1.31 0.690 0.192	1.38 0.68 0.200

TABLE I: Drag coefficient C_D , Lift coefficient C_L and Strouhal number St values for the Re=200 case.

present work and the literature result is obtained.

The same test cases have been solved using a uniform resolution equal to $D/\Delta x=100$ to assess if the variable resolution approach proposed here introduces any additional inconsistency. In Figure 5 the lift coefficient obtained using a uniform resolution is practically superimposed with the variable resolution, demonstrating the robustness of the approach. In the simulation with variable resolution, the total number of particles is equal to 1.31×10^2 , whereas the simulation with uniform resolution requires 5.04×10^6 .

2) Flow past an impulsively started cylinder at Re=9500: The same geometry is tested considering Reynolds Numbers equal to 9500. This flow has been investigated both experimentally [34] and numerically [35]. The simulation setup is similar to the previous case, while the velocity and density fields are initialized with a potential flow solution.

In comparison with the previous case for Re=200, this flow is characterized by a complex interaction between primaries and secondary vortex in the boundaries layer. In fact, primary vortexes form and detach from the cylinder, resulting in an high unsteadiness that affect the time history of the drag coefficient. A convergence study is performed, considering maximum resolutions equal to $\Delta x_{min}=800,1600,3200$ near the cylinder, which corresponds respectively to 6, 7, and 8 different resolution zones in the entire domain. In Figure 6 the drag coefficient is plotted against time for the three different resolution near the cylinder. Whereas all three simulations capture the drag coefficient until t=4, only the one with $\Delta x_{min}=3200$ is capable of reproducing the

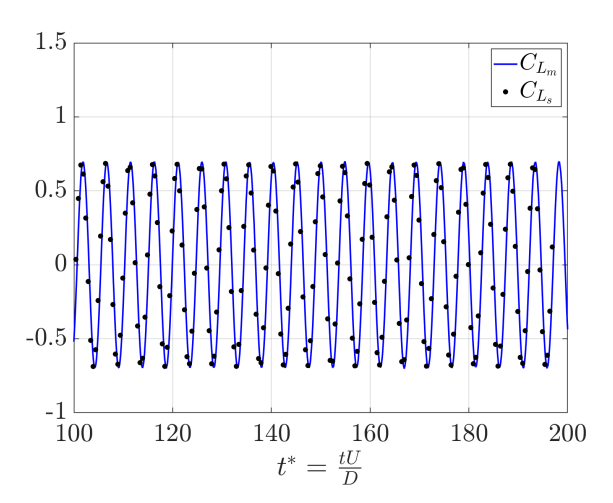


Fig. 5: Comparison of the time history of the lift coefficient for a flow past cylinder with Re=200 using a uniform and a variable resolution approach.

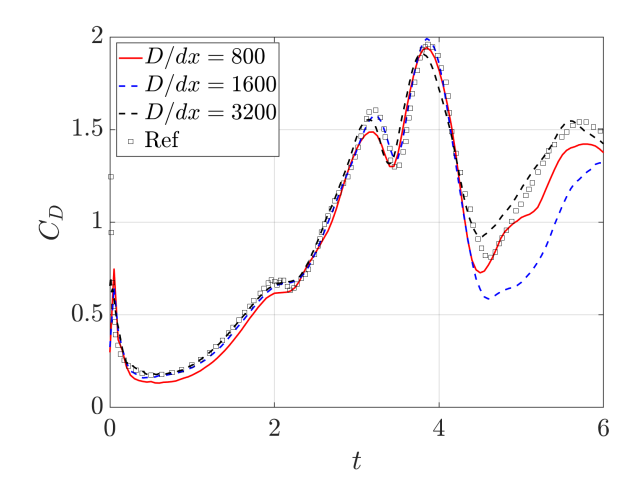


Fig. 6: Drag coefficient for an impulsively started cylinder with Re=9500. The numerical solution is compared with results in [35]

reference solution for t>4 when the flow is characterized by a high unsteadiness. Moreover, with higher resolution, the flow remains almost perfectly symmetrical as in the reference solution [35], as visible in Figure 7, where the vorticity contours for $t*=tU_{\infty}/D$ are shown. It is remarked that the multi-resolution approach simulation with $\Delta x_{min}=3200$ requires 8 sub-domains, resulting in a number of particles $N\approx 10\times 10^6$ which can be simulated using 1 GPU, while with a uniform resolution, the particles required with the same resolution would be $N\approx 9\times 10^9$ which can be achieved only with sophisticated memory-distributed parallelization [36].

B. Forced Cylinder

The flow past a cylinder moving transversally to the streamwise direction is investigated for a Re=100 with different frequencies and amplitudes. The present test case has been

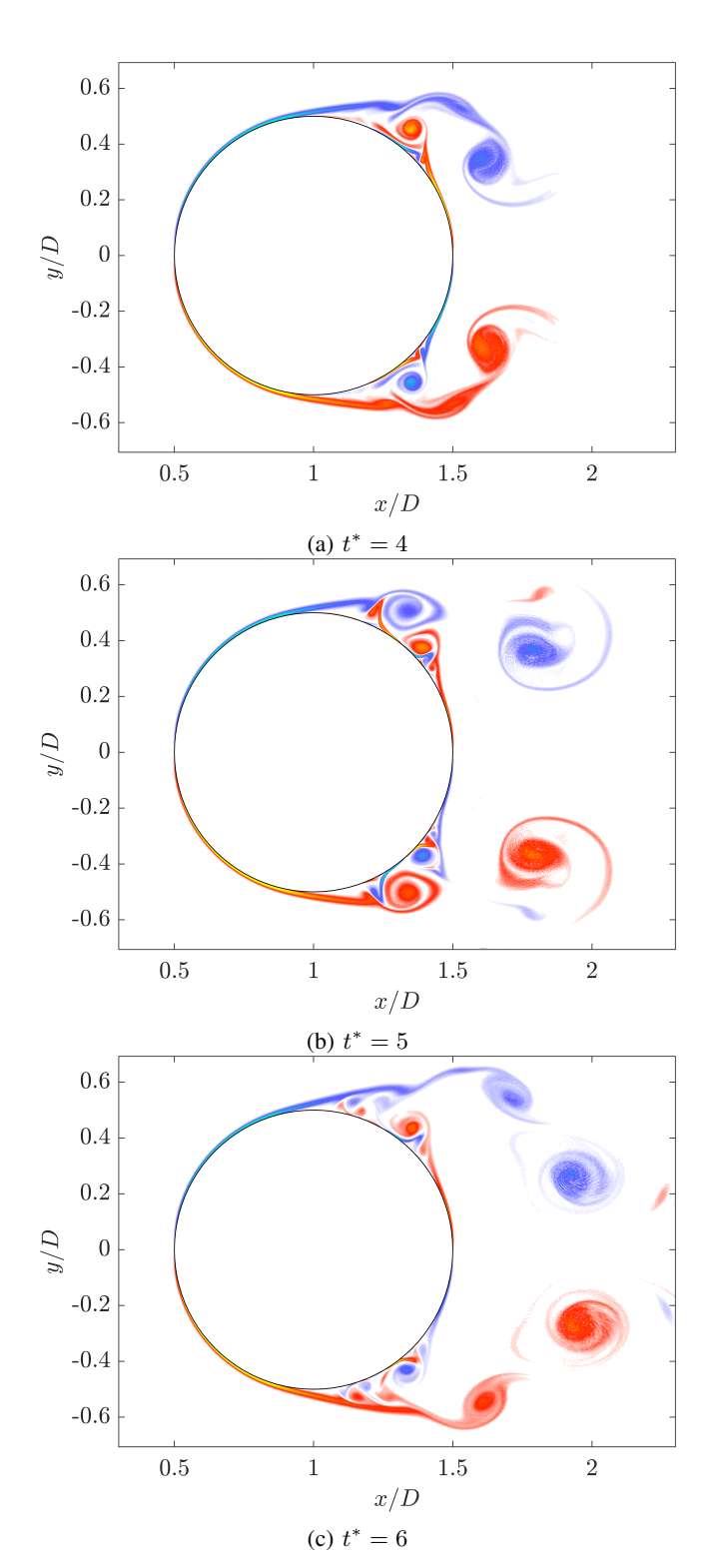


Fig. 7: Vorticity contours for a impusively started cylinder at Re=9500.

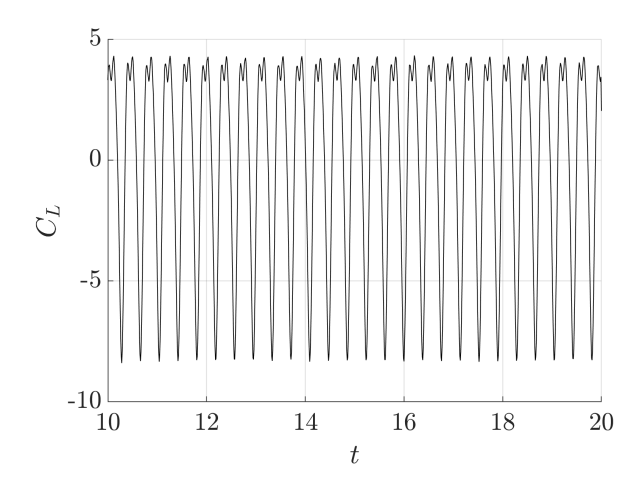


Fig. 8: Time history for the lift coefficient for the flow past an oscillating cylinder at Re=100 for (A, F) = (1.25, 1.5).

chosen in order to assess the capability of the proposed variable-resolution scheme to simulate flows with moving boundaries. This complex flow has been investigated by different researchers either numerically [37] or experimentally [38], [39]. The computational setup is the same as the one employed for studying the fixed cylinder case, and the domain has been discretized with three different resolution zones with particle sizes respectively equal to $D/\Delta x = 25, 50, 100$ with the highest resolution located near the cylinder.

A sinusoidal motion y(t) is applied to the cylinder in the crossflow direction:

$$y(t) = ADsin(2\pi F f_s t) \tag{11}$$

where $A=y_{max}/D$, with y_{max} equal to the maximum displacement and $F=f_0/f_s$ where f_s is the frequency of the vortex shedding when the cylinder remains fixed. As for the refinement regions, they both move according to Equation 11.

The case simulates a challenging configuration obtained by setting the coefficient pair equal to (A,F)=(1.25,1.5). Figure 8 shows the time history of the lift coefficient, whereas the Power Spectral Density (PSD) for the same quantity is shown in Figure 9. It can be noted a dominant frequency equal to $f=f_0$, coupled with a second and a third frequency at $f=2f_0$ and $f=3f_0$, in accordance with the results in [37]. These small secondary frequencies are not associated with the beating phenomena [37], but they influence the vortex shedding pattern, resulting in a pair plus single vortex configuration, as can be seen in Figure 10, where the dimensionless vorticity contours are shown.

C. Propagation of regular waves

To demonstrate the ability of the present variable resolution approach in treating free-surface flows, the propagation of waves is hereby investigated. The computational domain depicted in Figure 11 consists of a rectangular tank with

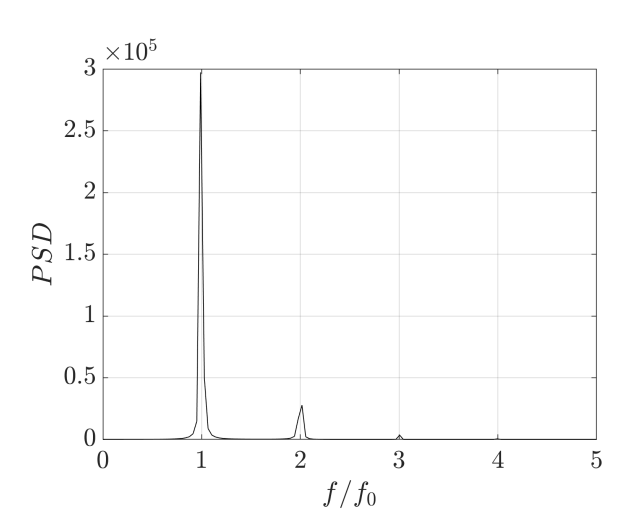


Fig. 9: Power Spectral Density (PSD) for the flow past an oscillating cylinder at Re=100 for (A, F) = (1.25, 1.5).

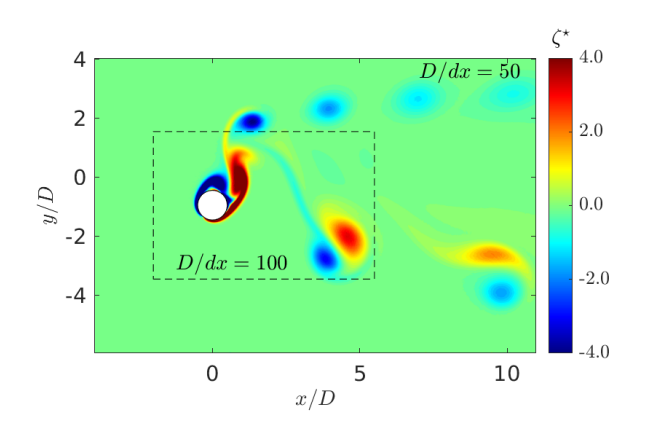


Fig. 10: Dimensionless vorticity contours for the flow past an oscillating cylinder at Re=100 for (A,F)=(1.25,1.5).

length L=16m filled by water with a level $d_1=0.66m$. Following the Stokes 2nd order wave theory, a piston-type wave-maker generates a train of regular waves with height H=0.2m and period T=2s for a total simulation time of t=80s, which gives approximately 40 waves throughout the simulation. The domain has been divided into two zones with different resolutions, and a dissipative region is placed at the right end of the domain to suppress wave reflection as shown in Figure 11 .

Following the indications in [40], which prescribed at least



Fig. 11: Computational domain for the propagation of regular waves case.

10 particles to describe a wavefront, particle spacing equal to $\Delta x = 0.01m$ is adopted in the left part of the domain (0m < x < 5m). In the region 2.5m < x < L a resolution equal to $\Delta x = 0.005m$ has been adopted. The multi-resolution simulation is compared with a second solution, obtained with a uniform particle spacing $\Delta x = 0.005m$. For the discretization of the viscous term in the governing equation, the artificial viscosity formulation is preferred with $\alpha = 0.02$, and the smoothing length to particle spacing ratio is set to $h/\Delta x = 2$. To measure the free-surface elevation and the orbital velocity, a wave gauge (WG) is placed respectively at x = 6.5m, at a height $d_v = 0.5m$.

In Figure 12 a comparison between multi and uniform-resolution formulations (with resolution $\Delta x = 0.005m$) is shown, demonstrating that the multi-resolution simulation results are in agreement with the ones obtained with a single resolution. Moreover, in Figures 12b and 12c also the orbital velocities are compared for the wave gauge at x = 6.5m, and also for the velocity the results are overall in good agreement. From the snapshot in Figure 13 for the density and the horizontal velocity, it can be seen that aren't visible any discontinuities at the interface between the two sub-domain, demonstrating once again the ability of the present algorithm to transmit accurately waves between sub-domains.

Finally, thanks to the absence of open boundary conditions, this test case allows some considerations on the mass conservation properties of the proposed approach. In Figure 14 is shown the time history of the mass for the multi-resolution simulation: despite the fact that the present approach doesn't enforce strict mass conservation, it can be seen that the mass variation in the total simulation is kept below the 0.03%.

V. Conclusions

In the present work, a novel approach to introduce variable resolution in SPH has been presented and implemented in the DualSPHysics open-source code. This approach is based on the partitioning of the computational domain into sub-domains. Each sub-domain is characterized by its own particle size, and the computational sub-problems are closed by buffer regions that act as Dirichlet boundary conditions. The proposed algorithm has been tested against different 2-D cases. The results demonstrate the ability to reduce by several orders of magnitude the computational cost associated with the number of particles without introducing any inaccuracies. Moreover, the present formulation is able to link the geometrical definition of the refinement regions to a moving object, and also to treat free-surface flows, keeping the competitive features of the SPH particle formulation with respect to grid-based methods. Future works will be focused on the extension and the validation to 3-D flows in DualSPHysics.

VI. ACKNOWLEDGEMENT

This material is based upon work supported by the National Science Foundation under Grant No. 2209793 and by the General Motors Company under Grant No. GAC3794.

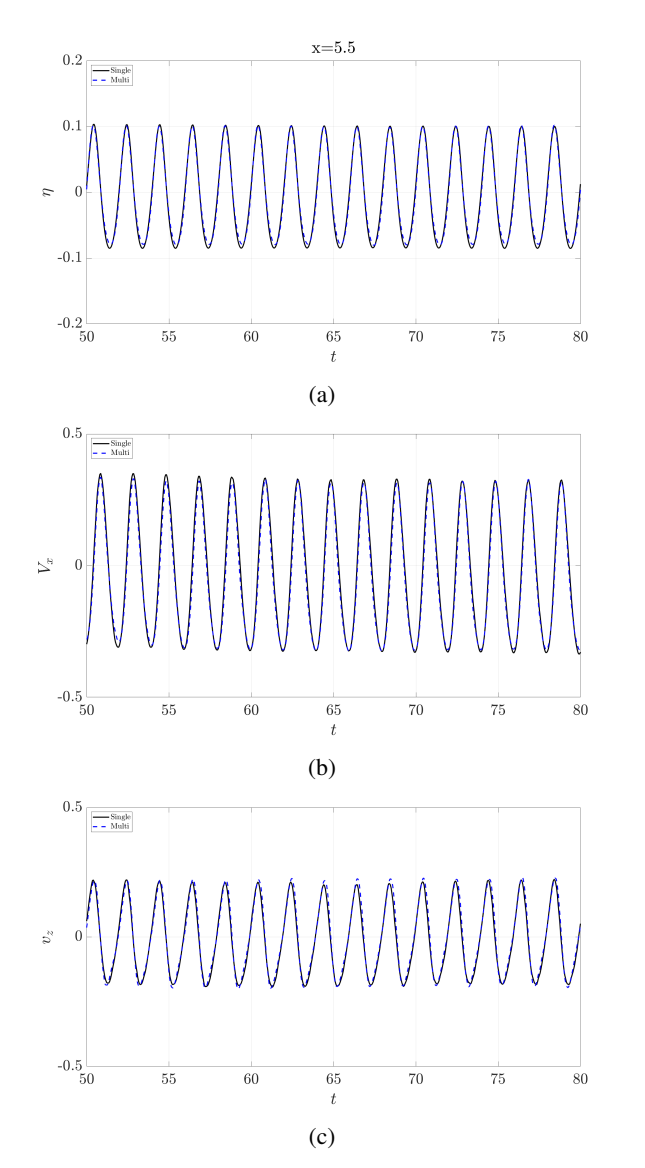


Fig. 12: Comparison of free-surface elevation and orbital velocity between a multi-resolution and uniform resolution simulation for the wave propagation test case.

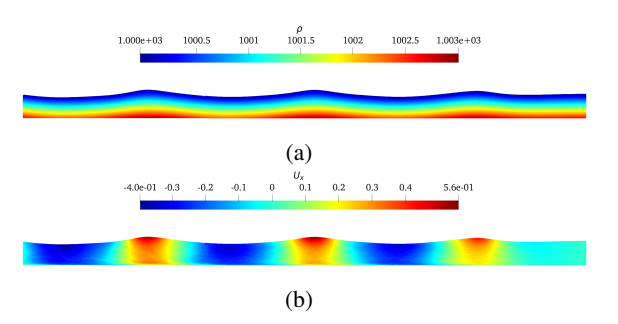


Fig. 13: (a) Density and (b) velocity contours for the multi-resolution simulation for the wave propagation test case.

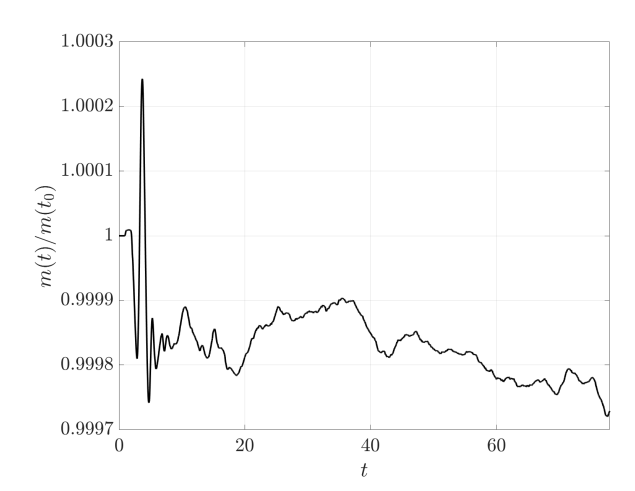


Fig. 14: Time history of the mass variation in the multiresolution simulation.

REFERENCES

- [1] R. Vacondio, C. Altomare, M. De Leffe, X. Hu, D. Le Touzé, S. Lind, J.-C. Marongiu, S. Marrone, B. D. Rogers, and A. Souto-Iglesias, "Grand challenges for smoothed particle hydrodynamics numerical schemes," *Computational Particle Mechanics*, vol. 8, no. 3, pp. 575–588, 2021.
- [2] J. M. Domínguez, G. Fourtakas, C. Altomare, R. B. Canelas, A. Tafuni, O. García-Feal, I. Martínez-Estévez, A. Mokos, R. Vacondio, A. J. Crespo et al., "Dualsphysics: from fluid dynamics to multiphysics problems," *Computational Particle Mechanics*, pp. 1–29, 2021.
- [3] R. A. Gingold and J. J. Monaghan, "Smoothed particle hydrodynamics: theory and application to non-spherical stars," *Monthly notices of the* royal astronomical society, vol. 181, no. 3, pp. 375–389, 1977.
- [4] D. Violeau and B. D. Rogers, "Smoothed particle hydrodynamics (sph) for free-surface flows: past, present and future," *Journal of Hydraulic Research*, vol. 54, no. 1, pp. 1–26, 2016.
- [5] Z.-B. Wang, R. Chen, H. Wang, Q. Liao, X. Zhu, and S.-Z. Li, "An overview of smoothed particle hydrodynamics for simulating multiphase flow," *Applied Mathematical Modelling*, vol. 40, no. 23-24, pp. 9625–9655, 2016.
- [6] A.-m. Zhang, P.-n. Sun, F.-r. Ming, and A. Colagrossi, "Smoothed particle hydrodynamics and its applications in fluid-structure interactions," *Journal of Hydrodynamics, Ser. B*, vol. 29, no. 2, pp. 187–216, 2017.
- [7] S. Osher and R. P. Fedkiw, "Level set methods: an overview and some recent results," *Journal of Computational physics*, vol. 169, no. 2, pp. 463–502, 2001.
- [8] V. R. Gopala and B. G. van Wachem, "Volume of fluid methods for immiscible-fluid and free-surface flows," *Chemical Engineering Journal*, vol. 141, no. 1-3, pp. 204–221, 2008.
- [9] S. O. Unverdi and G. Tryggvason, "A front-tracking method for viscous, incompressible, multi-fluid flows," *Journal of computational physics*, vol. 100, no. 1, pp. 25–37, 1992.
- [10] J. Bonet and M. X. Rodríguez-Paz, "Hamiltonian formulation of the variable-h sph equations," *Journal of Computational Physics*, vol. 209, no. 2, pp. 541–558, 2005.
- [11] G. Oger, M. Doring, B. Alessandrini, and P. Ferrant, "Two-dimensional sph simulations of wedge water entries," *Journal of computational physics*, vol. 213, no. 2, pp. 803–822, 2006.
- [12] P. Omidvar, P. K. Stansby, and B. D. Rogers, "Wave body interaction in 2d using smoothed particle hydrodynamics (sph) with variable particle mass," *International Journal for Numerical Methods in Fluids*, vol. 68, no. 6, pp. 686–705, 2012.
- [13] —, "Sph for 3d floating bodies using variable mass particle distribution," *International Journal for Numerical Methods in Fluids*, vol. 72, no. 4, pp. 427–452, 2013.
- [14] J. Feldman and J. Bonet, "Dynamic refinement and boundary contact forces in sph with applications in fluid flow problems," *International*

- Journal for Numerical Methods in Engineering, vol. 72, no. 3, pp. 295–324, 2007.
- [15] Y. Reyes López, D. Roose, and C. Recarey Morfa, "Dynamic particle refinement in sph: application to free surface flow and non-cohesive soil simulations," *Computational Mechanics*, vol. 51, no. 5, pp. 731–741, 2013.
- [16] R. Vacondio, B. D. Rogers, P. Stansby, P. Mignosa, and J. Feldman, "Variable resolution for sph: a dynamic particle coalescing and splitting scheme," *Computer Methods in Applied Mechanics and Engineering*, vol. 256, pp. 132–148, 2013.
- [17] R. Vacondio, B. D. Rogers, P. K. Stansby, and P. Mignosa, "Variable resolution for sph in three dimensions: Towards optimal splitting and coalescing for dynamic adaptivity," *Computer Methods in Applied Mechanics and Engineering*, vol. 300, pp. 442–460, 2016.
- [18] D. A. Barcarolo, D. Le Touzé, G. Oger, and F. De Vuyst, "Adaptive particle refinement and derefinement applied to the smoothed particle hydrodynamics method," *Journal of Computational Physics*, vol. 273, pp. 640–657, 2014.
- [19] L. Chiron, G. Oger, M. De Leffe, and D. Le Touzé, "Analysis and improvements of adaptive particle refinement (apr) through cpu time, accuracy and robustness considerations," *Journal of Computational Physics*, vol. 354, pp. 552–575, 2018.
- [20] P. Sun, A. Colagrossi, S. Marrone, M. Antuono, and A. Zhang, "Multi-resolution delta-plus-sph with tensile instability control: Towards high reynolds number flows," *Computer Physics Communications*, vol. 224, pp. 63–80, 2018.
- [21] X. Bian, Z. Li, and G. E. Karniadakis, "Multi-resolution flow simulations by smoothed particle hydrodynamics via domain decomposition," *Journal of Computational Physics*, vol. 297, pp. 132–155, 2015.
- [22] C. Zhang, M. Rezavand, and X. Hu, "A multi-resolution sph method for fluid-structure interactions," *Journal of Computational Physics*, vol. 429, p. 110028, 2021.
- [23] A. Khayyer, Y. Shimizu, H. Gotoh, and S. Hattori, "Multi-resolution isph-sph for accurate and efficient simulation of hydroelastic fluidstructure interactions in ocean engineering," *Ocean Engineering*, vol. 226, p. 108652, 2021.
- [24] A. Tafuni, J. Domínguez, R. Vacondio, and A. Crespo, "A versatile algorithm for the treatment of open boundary conditions in smoothed particle hydrodynamics gpu models," *Computer methods in applied mechanics and engineering*, vol. 342, pp. 604–624, 2018.
- [25] M. Liu and G. Liu, "Restoring particle consistency in smoothed particle hydrodynamics," Applied Numerical Mathematics, vol. 56, no. 1, pp. 19–36, 2006. [Online]. Available: https://www.sciencedirect.com/science/article/pii/S0168927405000565
- [26] H. Wendland, "Piecewise polynomial, positive definite and compactly supported radial functions of minimal degree," Advances in computational Mathematics, vol. 4, no. 1, pp. 389–396, 1995.
- [27] G. Fourtakas, J. M. Dominguez, R. Vacondio, and B. D. Rogers, "Local uniform stencil (lust) boundary condition for arbitrary 3d boundaries in parallel smoothed particle hydrodynamics (sph) models," vol. 190, pp. 346–361, 2019. [Online]. Available: https://www.sciencedirect.com/science/article/pii/S0045793019301859
- [28] S. Shao and E. Y. Lo, "Incompressible sph method for simulating newtonian and non-newtonian flows with a free surface," Advances in Water Resources, vol. 26, no. 7, pp. 787–800, 2003. [Online]. Available: https://www.sciencedirect.com/science/article/pii/S0309170803000307
- [29] A. English, J. Domínguez, R. Vacondio, A. Crespo, P. Stansby, S. Lind, L. Chiapponi, and M. Gómez-Gesteira, "Modified dynamic boundary conditions (mdbc) for general-purpose smoothed particle hydrodynamics (sph): Application to tank sloshing, dam break and fish pass problems," Computational Particle Mechanics, vol. 9, no. 5, pp. 1–15, 2022.
- [30] S. Marrone, A. Colagrossi, M. Antuono, G. Colicchio, and G. Graziani, "An accurate sph modeling of viscous flows around bodies at low and moderate reynolds numbers," *Journal of Computational Physics*, vol. 245, pp. 456–475, 2013.
- [31] S. Lind, R. Xu, P. Stansby, and B. Rogers, "Incompressible smoothed particle hydrodynamics for free-surface flows: A generalised diffusion-based algorithm for stability and validations for impulsive flows and propagating waves," *Journal of Computational Physics*, vol. 231, no. 4, pp. 1499–1523, 2012. [Online]. Available: https://www.sciencedirect.com/science/article/pii/S0021999111006279
- [32] B. J. Leimkuhler, S. Reich, and R. D. Skeel, "Integration methods

- for molecular dynamics," in *Mathematical Approaches to biomolecular structure and dynamics*. Springer, 1996, pp. 161–185.
- [33] C. Liu, X. Zheng, and C. Sung, "Preconditioned multigrid methods for unsteady incompressible flows," *Journal of Computational physics*, vol. 139, no. 1, pp. 35–57, 1998.
- [34] R. Bouard and M. Coutanceau, "The early stage of development of the wake behind an impulsively started cylinder for 40; re; 104," *Journal of Fluid Mechanics*, vol. 101, no. 3, pp. 583–607, 1980.
 [35] P. Koumoutsakos and A. Leonard, "High-resolution simulations of the
- [35] P. Koumoutsakos and A. Leonard, "High-resolution simulations of the flow around an impulsively started cylinder using vortex methods," *Journal of Fluid Mechanics*, vol. 296, pp. 1–38, 1995.
- [36] J. Domínguez, A. Crespo, D. Valdez-Balderas, Gómez-Gesteira, and M. "New multi-gpu implementation for smoothed particle hydrodynamics heteroge-Physics Communications, neous clusters." Computer 184. no. 8, pp. 1848-1860, 2013. [Online]. Available: https://www.sciencedirect.com/science/article/pii/S0010465513001057
- [37] A. Placzek, J.-F. Sigrist, and A. Hamdouni, "Numerical simulation of an oscillating cylinder in a cross-flow at low reynolds number: Forced and free oscillations," *Computers & Fluids*, vol. 38, no. 1, pp. 80–100, 2009.
- [38] J. Carberry, J. Sheridan, and D. Rockwell, "Forces and wake modes of an oscillating cylinder," *Journal of Fluids and Structures*, vol. 15, no. 3-4, pp. 523–532, 2001.
- [39] ——, "Controlled oscillations of a cylinder: forces and wake modes," Journal of Fluid Mechanics, vol. 538, pp. 31–69, 2005.
- [40] C. Altomare, J. M. Domínguez, A. Crespo, J. González-Cao, T. Suzuki, M. Gómez-Gesteira, and P. Troch, "Long-crested wave generation and absorption for sph-based dualsphysics model," *Coastal Engineering*, vol. 127, pp. 37–54, 2017.